

CHAPTER 5

TRANSFERS TO THE LUNAR SURFACE

5.1 EXECUTIVE SUMMARY

In this chapter techniques are developed that allow an analysis of a range of different types of transfer trajectories from the Earth to the lunar surface. Trajectories ranging from those obtained using the invariant manifolds of unstable orbits to those derived from collision orbits are analyzed. These techniques allow the computation of trajectories encompassing low-energy trajectories as well as more direct transfers. A conceptual illustration of the types of trajectories discussed in this chapter is given in Fig. 5-1. The range of possible trajectory options is summarized, and a broad range of trajectories that exist as a result of the Sun's influence are computed and analyzed. The results are classified by type, and trades between different measures of cost are discussed. The information in this chapter is largely derived from papers presented by Anderson and Parker [192–195], and the results as presented here are oriented as a guide for mission design.

The problem of designing transfers to the lunar surface is approached here as follows. First, an analysis is given showing the types of trajectories that exist as a result of the Sun's influence in both the planar and spatial problems. A significant set of trajectories at high Jacobi constants, or low energies, is found to exist when the Sun's

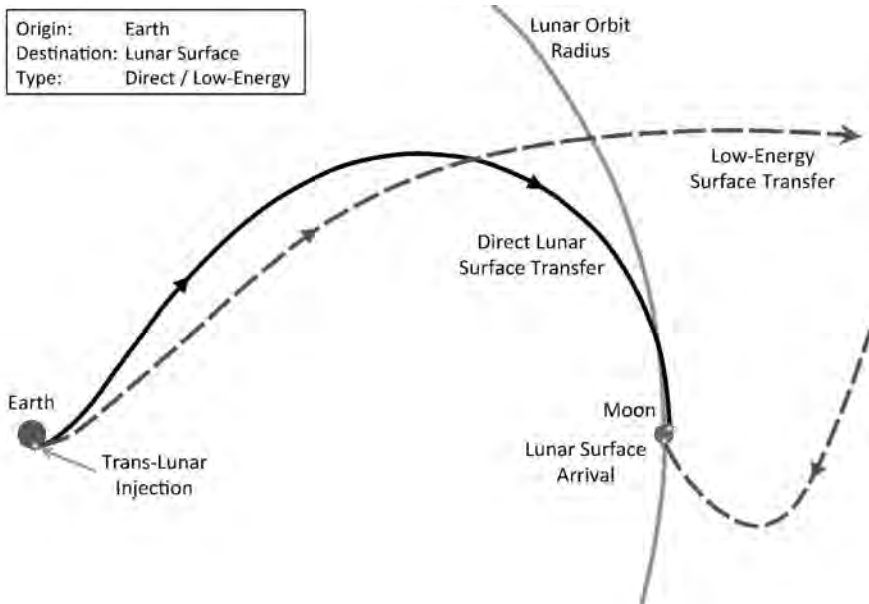


Figure 5-1 The profiles for both a direct and a low-energy transfer from the Earth to the lunar surface.

influence is taken into account. This result indicates that for trajectory design in this energy regime, trajectories traveling to the Sun–Earth Lagrange points and following the invariant manifolds of orbits around these points deserve careful consideration. Monthly variations are examined, and it is determined that the monthly variations capture the majority of the variations seen in the studied transfer trajectories. The greatest variation over a month occurs between the cases traveling to the Moon when it is at its apoapse and periapse. These trajectories are described for the spatial case initially with trajectories normal to the surface, which illustrates in a succinct manner the types of options available. A more detailed analysis of trajectories arriving at various angles to the surface is also presented, and these trajectory options are summarized using several different plots of various parameters. These trajectories may serve as initial guesses for future mission design, and they provide a general overview of the range of trajectory options. Invariant manifold trajectories traveling to the lunar surface are also described, and some sample trajectory options traveling from libration orbits to the lunar surface are given.

The numerical results presented in this chapter are given primarily relative to the Jacobi constant (C) of trajectories encountering the lunar surface. The velocity of the trajectories varies little over the surface of the Moon for each Jacobi constant, and in each case an approximate value of the velocity corresponding to each Jacobi constant may be obtained by referring to Fig. 5-2. From this plot, a Jacobi constant of 2.5 gives

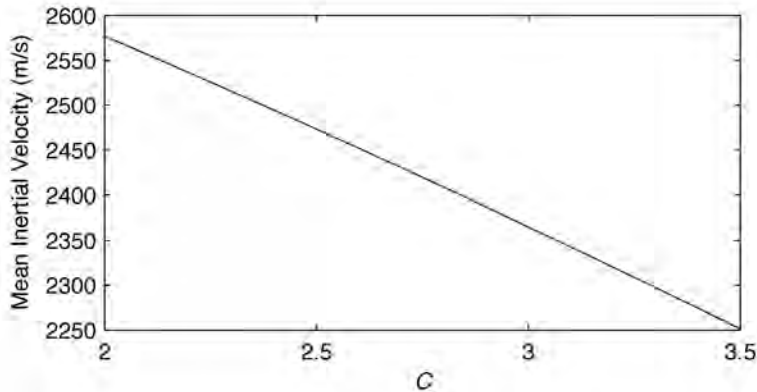


Figure 5-2 Mean inertial velocities relative to the Moon at each Jacobi constant for the cases with velocities normal to the surface [192] (Copyright © 2011 by American Astronautical Society Publications Office, San Diego, California (Web Site: <http://www.univelt.com>), all rights reserved; reprinted with permission of the AAS).

a mean velocity at the Moon of approximately 2473.3 meters per second (m/s), while a Jacobi constant of 3.0 gives a mean velocity of 2365.0 m/s. In the planar analysis it is shown that trajectories from the Earth to the Moon exist without the Sun's influence up to a Jacobi constant of 2.78, while they exist up to a Jacobi constant of 3.16 when the Sun's influence is included in the computations. As expected, the time of flight of the trajectories generally increased and the launch injection energy parameter (C_3) generally decreased as the Jacobi constant increased. For the spatial case with trajectories encountering the Moon perpendicular to the surface, the minimum time of flight varied from approximately 3.4 days at $C = 2.2$ to around 101.0 days and 78.7 days at $C = 3.0$ and 3.1, respectively. The range of possible elevation angles that generate missions to the surface is very dependent on the Jacobi constant and the target location on the surface. For the selected grid size, the maximum elevation angle range for points on the surface changed from 0 deg to 90 deg at $C = 2.6$ to between 57 deg and 90 deg at $C = 3.1$. Likewise the minimum elevation angle range decreased from 0 deg to 72 deg at $C = 2.6$ to between 0 deg and 15 deg at $C = 3.1$. These numbers are given to present a rough idea of the kinds of results that are discussed in this chapter. The details of these cases along with a wide variety of launch and approach parameters are contained in the plots presented throughout the chapter.

5.2 INTRODUCTION FOR TRANSFERS TO THE LUNAR SURFACE

A wide variety of Earth–Moon trajectories have been employed for past missions, ranging from the more direct transfers used for the Apollo missions [196] to more recent missions such as *ARTEMIS* [4] that make use of the multi-body dynamics

of the Earth–Moon and Sun–Earth–Moon systems. The design of trajectories in multi-body systems is a particularly rich problem because the two-body model is often insufficient to compute accurate trajectories, and the gravity of the Sun, Earth, and Moon combine to form a highly nonlinear dynamical environment. These facts limit the applicability of traditional patched-conic techniques commonly used for interplanetary missions, and the three-dimensional aspects of the problem further complicate real-world missions. Mission designers must take into account the orientation of each body in addition to the relative orientations of the orbits of the Earth and the Moon over time. Parker et al. [44, 47, 183] have studied trajectories that include many of these complicating factors for insertion into a variety of orbit types near the Moon. This chapter focuses on an analysis including these types of effects with a focus on trajectories traveling to the lunar surface.

Lunar landing trajectories often have a different set of constraints from those of orbiters, and the nature of this problem makes it possible to approach it with a different set of techniques. Indeed, a theoretical basis for analyzing lunar landing trajectories may be found in the computation of collision orbits. Collision orbits have been studied extensively in the mathematical community by Easton [197] and McGehee [198]. Anderson and Lo [199], Villac and Scheeres [200], and Von Kirchbach et al. [201] have previously analyzed collision orbit trajectories for the Jupiter–Europa system and categorized the different regions and trajectories that exist for orbits that terminate or originate at Europa’s surface. While the theoretical basis for collision orbits is focused on trajectories that intersect the surface of the selected body normal to the surface, this type of analysis can be extended to trajectories coming in at the various flight path angles and declinations of interest to mission designers. A study of these trajectories is almost directly applicable to impactor missions such as the *Lunar Crater Observation and Sensing Satellite (LCROSS)* [202]. This mission used an 86 deg impact angle relative to the lunar surface for the impact trajectory. The techniques developed here are also easily applied to systems including the full ephemeris and multiple bodies. Much of the work to design low-energy trajectories from the Earth to the Moon has focused on the use of libration point orbits along with their stable and unstable manifolds [39, 45, 51, 203]. These techniques have proven to be quite successful, and they are increasingly used for the design of Earth–Moon trajectories. The invariant manifolds of libration orbit trajectories are also studied here with an emphasis on their applicability to landing trajectories.

A wide range of trajectory types for lunar landing trajectories were computed for the results given here, and presenting a complete picture of the possible trajectory categories while remaining easily accessible was a goal of this research. In keeping with this goal, the problem is approached and presented using several different levels of analysis with increasing complexity. Presenting all different combinations of velocities encountering the surface of the Moon with all different magnitudes and orientations makes it difficult to see the relevant structures in the solution space, so two divisions were made in the approach to the analysis. The problem is first approached by analyzing planar cases covering selected velocities or energies with the trajectories encountering the Moon at various angles relative to the surface. The characteristics of these trajectories are observed to lay the groundwork for understanding the spatial

trajectory cases. The spatial case is then attacked using the results from the planar analysis to understand the dynamics in this more complex model. These trajectories are categorized with the goal of providing a broad survey of the trajectory types that may be available for transfers to the lunar surface from the Earth. The specific trades between launch costs and time of flight (TOF) are quantified and summarized in addition to the topological characteristics of the trajectories. Other parameters relevant to mission design such as the launch orientation are computed. The regions of the Moon attainable using different types of trajectories are also characterized. These results are summarized with the goal of providing a tool for mission designers to quickly understand the trades between various measures of cost and time when a particular mission is being designed to land on the Moon.

The results in this chapter are also presented using two key concepts. The first is to view the problem in terms of the limiting bounds that a mission designer could use to refine the search space. This practically takes the form of computing parameters such as the velocities for which trajectories exist that travel from the Earth to the Moon or the launch energies required to reach such trajectories. The second, which is an overall theme of this work and one of the primary results, is related to computationally examining in a more comprehensive sense the trajectories available when the Sun's perturbations are taken into account. To achieve this objective, comparisons involving several different models are made. Many traditional trajectories were computed using the Earth–Moon model or the circular restricted three-body problem (CRTBP), and in general, similar types of trajectories exist in the full ephemeris model. If simpler models are used, however, some solutions in the full problem may be ignored. Some particular solutions employing the effects of the Sun for transfers in the Earth–Moon system have been examined more recently. The 1991 Japanese mission *MUSES-A (Hiten)* used the effects of the Earth, Moon, and Sun for its transfer to the Moon [30]. Koon et al. provided techniques for systematically reproducing missions similar to Hiten using the invariant manifolds of libration orbits [38]. In each of these techniques the Sun's effects were included in the mission design. Parker and Lo examined trajectories within the Sun–Earth–Moon spatial problem and looked at multiple trajectories for transfer to lunar halo orbits [39, 46]. The work here seeks to broaden the search space for landing trajectories traveling to the Moon and characterize the effects of the fourth-body perturbations of the Sun on the potential trajectories that may be used. A direct approach isolating the effects of the Sun is taken here by comparing trajectories in the CRTBP, the Earth–Moon system, and the Sun–Earth–Moon system.

5.3 METHODOLOGY

Two primary models are used for the analyses contained in this chapter. The first model, the CRTBP, closely approximates real world systems, and a significant set of tools exists within this model to bring to bear on the problem. The qualitative insights gained in this model are very helpful in providing an overview of the categories of trajectories that are available. The trajectories developed within the CRTBP are

also generally transferable to the full ephemeris although trajectories developed with the effects of other bodies may not be transferable to the CRTBP. Refer back to Section 2.5.1 for a more complete description of the CRTBP. The ephemeris model, implemented using point masses, is used to capture additional types of trajectories that are not found using the CRTBP model. Although the variations in the orbits of the Earth and Moon are important, this model is primarily used to search for members of the broad category of trajectories utilizing the Sun's perturbation for Earth–Moon transfers. See Section 2.5.3 for more details on the use of the ephemeris.

5.4 ANALYSIS OF PLANAR TRANSFERS BETWEEN THE EARTH AND THE LUNAR SURFACE

The procedure described next involves varying the location of the landing site on the Moon, the orientation of the incoming trajectory, and the energy/velocity of the trajectory. Each trajectory must also be characterized or evaluated using some figure of merit. While this can provide a relatively complete picture of the potential trajectory options, it is helpful to first gain insight into the dynamics by limiting the scope of the problem to allow the results to be easily visualized.

Several different techniques have been used to achieve this goal in the Jupiter–Europa system, and it is useful to consider their application here. One technique used by Anderson and Lo [199] varied the Jacobi constant for trajectories intersecting Europa on a sphere for several different trajectory orientations and characterized the origin of the trajectories. Von Kirchbach et al. [201] examined the planar case for the Jupiter–Europa system for additional velocity orientations leaving the surface. Both of these techniques are applied here to the Earth–Moon system, and it is interesting to start with the planar problem in order to gain some initial insight. First, the planar results are computed in the Earth–Moon CRTBP system to allow for a comparison with the results from Von Kirchbach et al. [201] in the Jupiter–Europa system. This technique is then used to extend the analysis to the ephemeris case with the Earth and Moon and then to the case where the Sun is included. The effect of adding the Sun is examined in detail over a range of Jacobi constants.

For this planar analysis, a set of trajectories was integrated backward in time from the surface of the Moon. Specifying the Jacobi constant gives the velocity magnitude for each trajectory, while the location of the trajectory and the orientation of the velocity are specified using α and θ as shown in Fig. 5-3. Multiple simulations have been performed using these techniques, and the results for several selected Jacobi constant values are given in Fig. 5-4. The resulting points are colored according to the original location of each trajectory. Note that if a trajectory integrated backward in time were to intersect the Moon and then encounter the Earth at an earlier time, the trajectory would be gray. The (α, θ) point corresponding to the intermediate intersection of the Moon would then be blue. The fact that points with only slightly different initial conditions in the plot can travel to either the Earth or the Moon confirms the known existence of chaos in this problem. Comparison with the results from the Jupiter–Europa system in Von Kirchbach et al. [201] reveals that the divid-

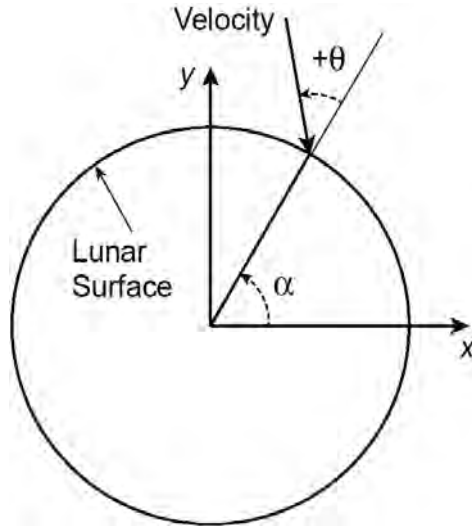


Figure 5-3 Diagram showing location and orientation of the velocity vector as it intersects the lunar surface. The xy axes shown here are centered on the Moon in the same orientation as the axes in the rotating frame [192] (Copyright © 2011 by American Astronautical Society Publications Office, San Diego, California (Web Site: <http://www.univelt.com>), all rights reserved; reprinted with permission of the AAS).

ing lines between different regimes of motion are less distinct at equivalent Jacobi constants for the Earth–Moon system. This existence of chaos indicates that it may be possible to design trajectories that cover a relatively wide range of the surface by carefully selecting landing sites. It is useful to note here again that Moon–Earth transfers may be derived from Earth–Moon transfers, and the plot corresponding to these trajectories may be obtained from Fig. 5-4 for the planar problem using $x \rightarrow x$, $y \rightarrow -y$, $\dot{x} \rightarrow -\dot{x}$, and $\dot{y} \rightarrow \dot{y}$. The transformation in position gives $\alpha \rightarrow 2\pi - \alpha$ and then from examination of the transformed velocity vector, $\theta \rightarrow -\theta$.

As can also be seen from the results, a significant percentage of the trajectories do not encounter either the primary or the secondary over the given time span. However, it is useful to note that for low Jacobi constants (higher energies), a significant percentage of the trajectories do originate at the Earth. Determining the Jacobi constant where Earth–Moon transfer trajectories no longer exist in the planar problem can help provide a rough limit on energies or velocities for these trajectories and provide a method for determining the potential benefits of perturbations from other bodies in trajectory design. To determine the approximate Jacobi constant above which Earth–Moon trajectories computed in this simulation no longer exist, a series of runs were made in parallel to step through the Jacobi constant. The grid resolution used for this step was one degree in both α and θ . The percent of the total number of trajectories that encountered the Earth for each Jacobi constant was computed and

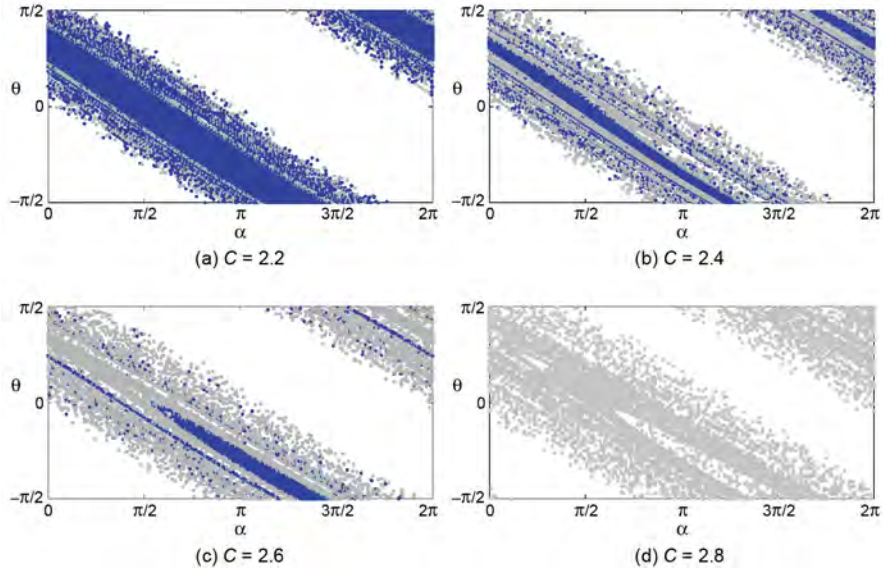


Figure 5-4 Plots showing the origin of each trajectory as a function of the position and orientation of the velocity vectors as the trajectories encounter the Moon's surface. Blue points indicate that the trajectory originated at the Earth and gray that it originated at the Moon. If no point is plotted the integrated trajectory did not encounter the surface of either body over the given time span of 200 days (Earth–Moon CRTBP) [192] (Copyright © 2011 by American Astronomical Society Publications Office, San Diego, California (Web Site: <http://www.univelt.com>), all rights reserved; reprinted with permission of the AAS). (See insert for color representation of this figure.)

plotted in Fig. 5-5. As expected from the previous plots, the number of trajectories originating at the Earth generally decreases with increasing Jacobi constant, but it is interesting that the slope of the curve varies significantly over the plotted range. It is also interesting that although the curve approaches zero percent near a Jacobi constant of 2.7, for Jacobi constants as high as 2.78, the percent of trajectories originating at the Earth remains at approximately 0.03 percent or approximately 19 out of 64800 trajectories. So even for this relatively low energy, some trajectories manage to travel from the Earth to the Moon.

For mission design, it is helpful to be aware of the velocities of the trajectories as they intersect the surface. They will actually vary somewhat as the constant for the computations so far has been the Jacobi constant rather than velocity. In general the inertial velocities relative to the Moon only vary at the m/s level. Figure 5-2 shows the average velocities for the case with velocities normal to the surface as a reference for each Jacobi constant.

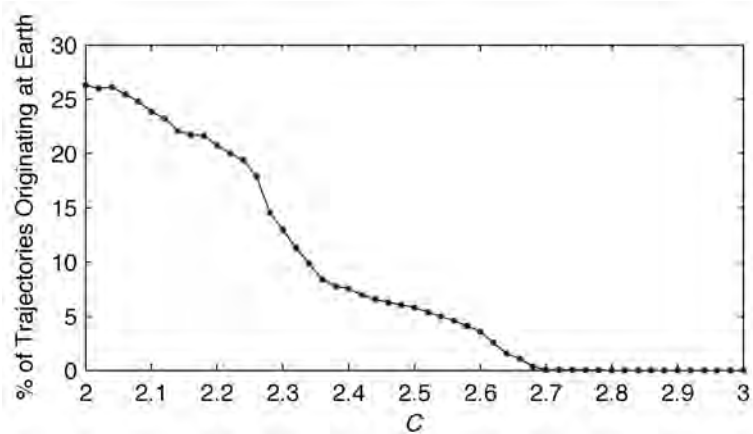


Figure 5-5 Percent of trajectories originating at the Earth for each Jacobi constant (CRTBP [192] (Copyright © 2011 by American Astronautical Society Publications Office, San Diego, California (Web Site: <http://www.univelt.com>), all rights reserved; reprinted with permission of the AAS).

Although the CRTBP is known to provide an accurate approximation to real-world trajectories, an obvious question for mission designers is related to how much the inclusion of real-world effects would affect selected trajectories. This question can be addressed by using planetary ephemerides and replicating the analysis for the CRTBP in this model. This analysis was first performed in the ephemeris model initially including only the gravity of the Earth and Moon. The initial velocities were computed for a given Jacobi constant in the CRTBP in the rotating frame, and then the states were initialized in the integrator relative to the Moon in an instantaneous rotating frame aligned with the Earth–Moon frame on an epoch of January 1, 2015. As the distance between the Earth and the Moon varies over the course of the orbit, it is difficult to obtain a direct comparison to the results from the CRTBP, but this method was selected because it was found to provide a good approximate comparison using the important mission design parameter of velocity at the lunar surface. Although the Jacobi constant will vary along the trajectory in this model, the final impact velocities at the Moon will be the same in each system. So the Jacobi constant labels in the ephemeris model plots in this study serve to indicate the velocities that were used at the lunar surface as they were computed in the CRTBP. The initial conditions were originally planar for this case, but the trajectory was free to vary in three dimensions for this problem. Using this method for a system including the Earth and Moon ephemerides, the trajectories were integrated, and the results are plotted in Fig. 5-6. Comparing the results for this system with the results in Fig. 5-4 reveals few obvious differences. The Earth impacting cases for $C = 2.6$ have some slight differences, but in general the trajectories match the expectation that the CRTBP is a good approximation to the three-body problem including the ephemerides. If the

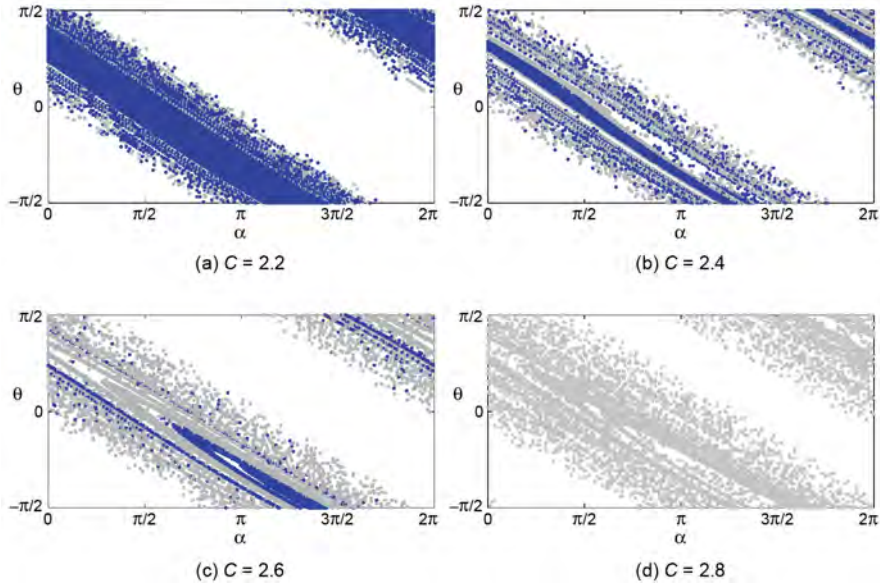


Figure 5-6 Plots showing the origin of each trajectory as a function of the position and orientation of the velocity vectors as the trajectories encounter the Moon. Blue points indicate that the trajectory originated at the Earth and gray that it originated at the Moon. If no point is plotted the integrated trajectory did not encounter either body over the given time span of 200 days (Earth–Moon only Ephemeris system) [192] (Copyright © 2011 by American Astronautical Society Publications Office, San Diego, California (Web Site: <http://www.univelt.com>), all rights reserved; reprinted with permission of the AAS). (See insert for color representation of this figure.)

percent of trajectories originating at the Earth are compared, some differences in the shape of the curve can be found, but the overall trends are very similar. In this case, the percent of trajectories in Fig. 5-7 originating at the Earth decreases down to 0.006 percent at $C = 2.76$, approximately the same Jacobi constant cutoff as the CRTBP.

Next, the same procedure was performed including the Sun in the integration, and the results are plotted in Fig. 5-8. Now, comparison with the results in both the CRTBP and the Earth–Moon systems reveal some obvious differences. Several new bands of trajectories originating at the Earth spring into existence. The overall structure remains generally similar, but the points appear chaotic. A new band of solutions remains for $C = 2.8$ and a significant number of Earth origin trajectories still exist at $C = 3.0$. Remember that the final velocities at the Moon are the same as the other models, but the Jacobi constant will vary as a result of the Sun's influence. In this sense, the Sun may be thought of as changing the trajectory's energy or Jacobi constant to provide the transfer. If the percent of trajectories originating at the Earth

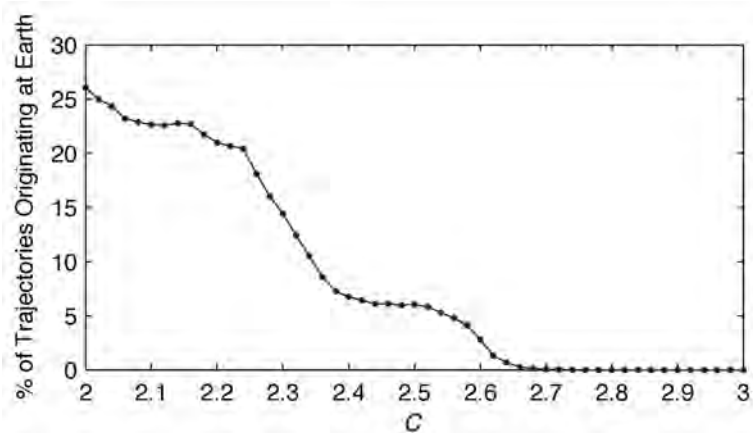


Figure 5-7 Percent of trajectories originating at the Earth for each Jacobi constant (Earth–Moon only Ephemeris system) [192] (Copyright © 2011 by American Astronautical Society Publications Office, San Diego, California (Web Site: <http://www.univelt.com>), all rights reserved; reprinted with permission of the AAS).

is examined in Fig. 5-9(a), it can be seen that at $C = 3.0$, 0.3 percent of the trajectories still originate at the Earth. Indeed, as high as $C = 3.16$, 0.15 percent of the trajectories still originate at Earth.

One immediate question that arises is whether the selected epoch for lunar arrival would significantly affect these results, so three additional cases seven days apart were computed and plotted in Fig. 5-9(b). Some variation is observed as the Moon travels through its orbit with one case starting with a lower percent of trajectories for low Jacobi constants and two of them possessing peaks just before $C = 3.0$. However, all of them have approximately the same upper Jacobi constant cutoff of approximately $C = 3.16$ where the percent of trajectories drops to near zero. The existence of the additional bands of trajectories and the increase in the Jacobi constant where trajectories connecting the Earth and Moon exist in this system raises the question as to where these trajectories come from. These trajectories were plotted in both the Earth–Moon system and the Sun–Earth–Moon system to examine the differences, and a sample of one of these trajectories plotted in both rotating frames is given in Fig. 5-10. As can be seen from the plots, the trajectory ends up in very different places depending on whether the Sun is included in the integration or not. In the Earth–Moon rotating frame with the Sun included, the trajectory travels far away from the system with no close periapses until it approaches the Earth, while the case without the Sun has two relatively close periapses at approximately the lunar distance and ends up far from the Earth. The most telling plots, however, are in the Sun–Earth rotating frame. Here, the characteristic shape of a trajectory using the libration point dynamics of the Sun–Earth system is apparent when the Sun is included. The trajectory travels out toward the L_1 point, lingers there, and then finally falls back

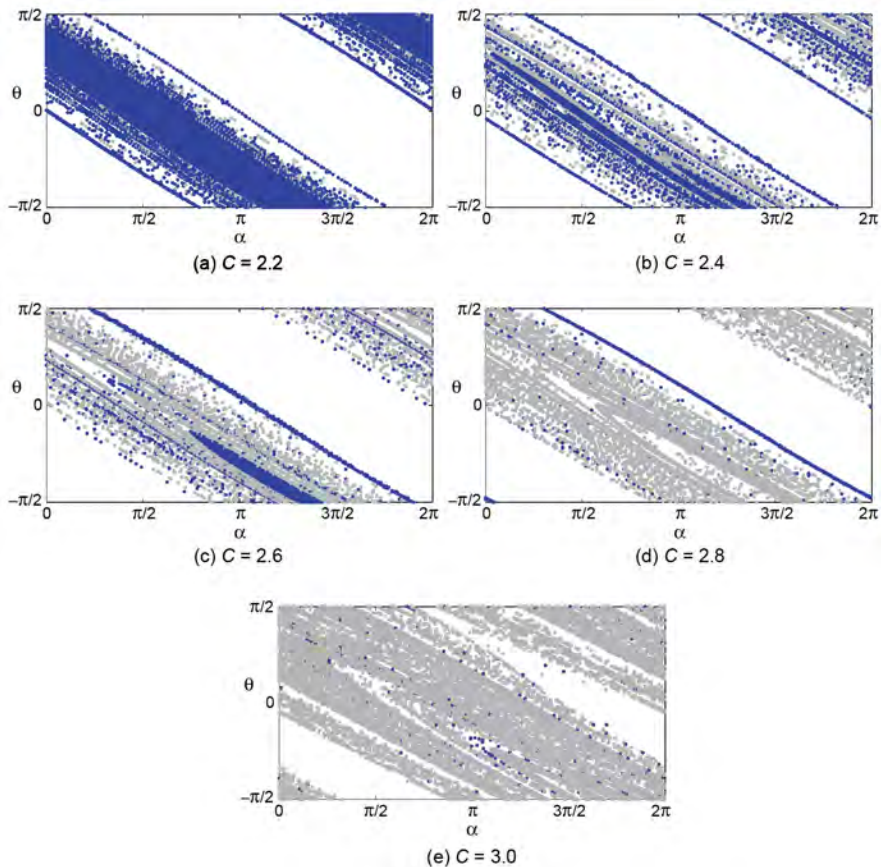


Figure 5-8 Plots showing the origin of each trajectory as a function of the position and orientation of the velocity vectors as the trajectories encounter the Moon. Blue points indicate that the trajectory originated at the Earth and gray that it originated at the Moon. If no point is plotted the integrated trajectory did not encounter either body over the given time span of 200 days (Sun–Earth–Moon Ephemeris system) [192] (Copyright © 2011 by American Astronautical Society Publications Office, San Diego, California (Web Site: <http://www.univelt.com>), all rights reserved; reprinted with permission of the AAS). (See insert for color representation of this figure.)

toward the Earth. Without the Sun, the trajectory stays out near the Moon until it eventually wanders further away from the system, unless there is a lunar flyby.

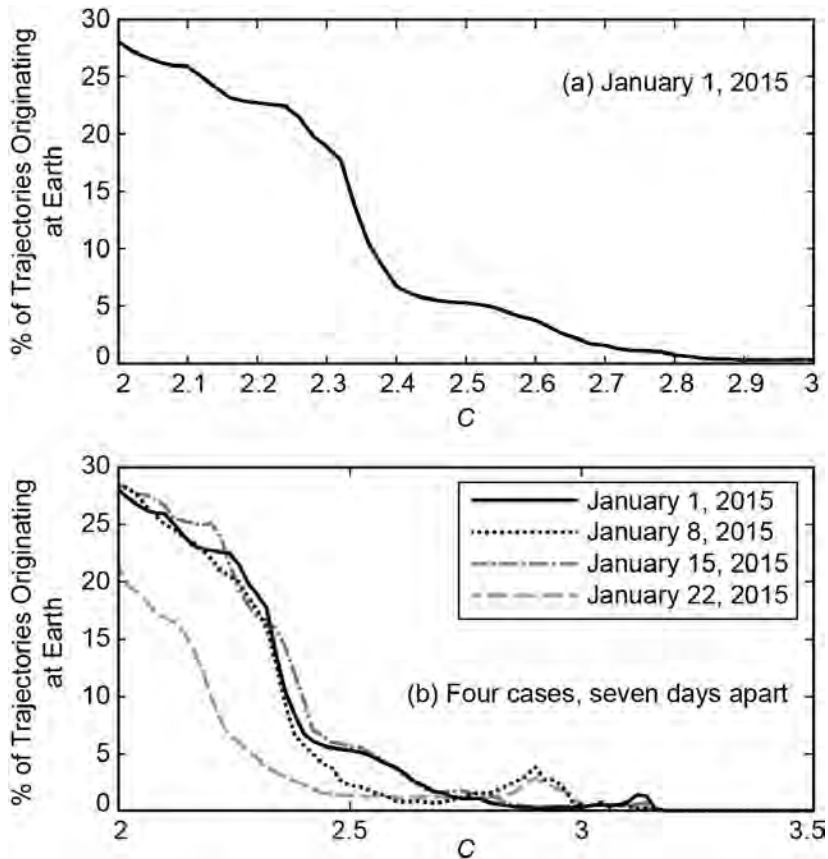


Figure 5-9 Percent of trajectories originating at the Earth for each Jacobi constant (Sun–Earth–Moon Ephemeris system) [192] (Copyright © 2011 by American Astronautical Society Publications Office, San Diego, California (Web Site: <http://www.univelt.com>), all rights reserved; reprinted with permission of the AAS).

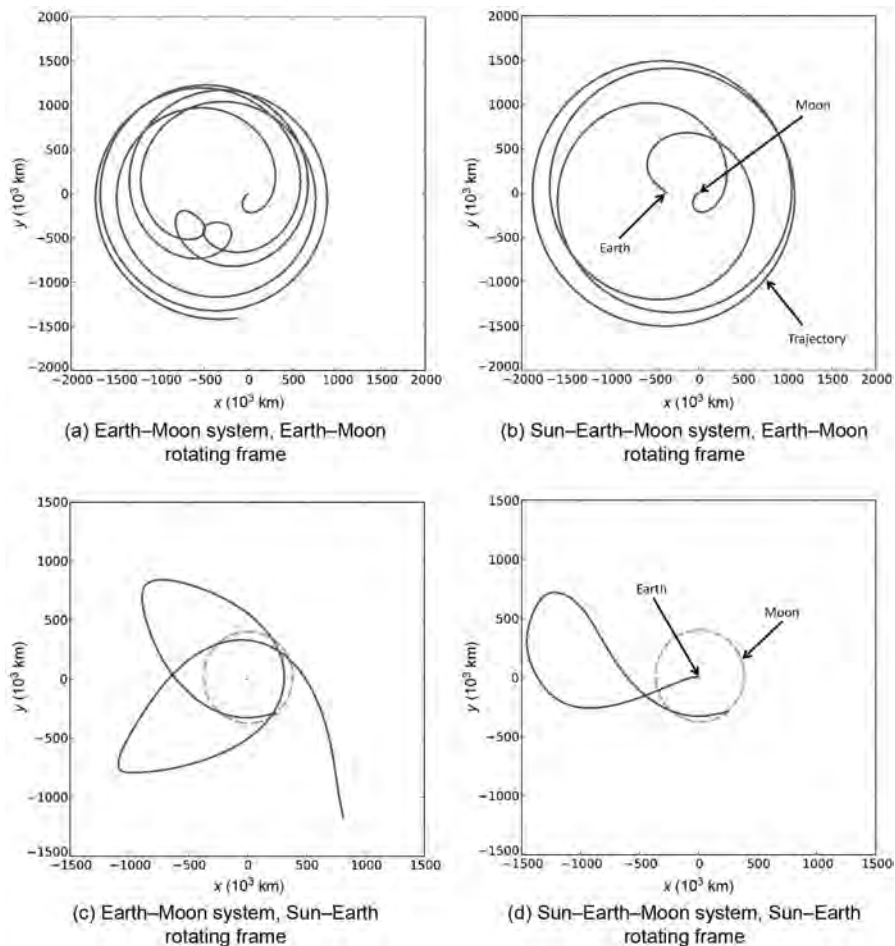


Figure 5-10 Comparison of a single trajectory at $C = 2.8$ ($\alpha \approx 197.5$ deg, $\theta \approx 9.5$ deg) integrated with and without the Sun's gravity in different rotating frames [192] (Copyright © 2011 by American Astronautical Society Publications Office, San Diego, California (Web Site: <http://www.univelt.com>), all rights reserved; reprinted with permission of the AAS).

5.5 LOW-ENERGY SPATIAL TRANSFERS BETWEEN THE EARTH AND THE LUNAR SURFACE

5.5.1 Trajectories Normal to the Surface

While the planar cases discussed up to this point are quite complicated, it is still possible to plot many of the salient features of the design space given the relatively small dimension of the problem. With the increase in dimension that occurs for the spatial problem, the visualization of the resulting trajectories and their characteristics becomes an even more difficult issue. One of the stated objectives of this analysis is to capture the characteristics of the major trajectory categories while also providing adequate information to evaluate the usefulness of each trajectory. With this objective in mind it is worth noting that if the plots in Figs. 5-4, 5-6, and 5-8 are examined, it can be seen that the majority of the dominant types of trajectories seen in the figures may be captured by making a particular cut at $\theta = 0$. The trajectories obtained with $\theta = 0$ correspond to those trajectories impacting the Moon normal to the lunar surface. As previously mentioned, these types of trajectories are particularly applicable to impactor missions similar to *LCROSS*. Given the results from the planar case, they can also provide a good initial overview of the different categories of Earth–Moon landing trajectories, including those with different flight path angles. The results presented next are restricted to those computed using impacts normal to the surface for an epoch of January 1, 2015. They provide accurate results for impactor-type trajectories, and they also give a good indication of the types of trajectories that may exist for trajectories coming in at other flight path angles.

To allow for easy visualization of the trajectory characteristics, the results are presented for each energy level, which corresponds to a slightly varying velocity magnitude relative to the Moon that depends on the location of the final point on the trajectory at the Moon's surface. The velocity can be used to provide an indication of the change in velocity (ΔV) required for landing, although the specific ΔV will depend on the particular landing trajectory. The regions of the Moon that are accessible for each energy level can be evaluated for particular mission design requirements by using the desired parameters plotted over the surface of the Moon in α and β . α and β are measured in the rotating frame with α positive in the same direction as shown in Fig. 5-3. β is measured like latitude and is positive above the xy plane. Understanding how to connect the trajectory to the Earth becomes more of a challenge in the spatial problem because a large number of possible Earth-relative orientations and methods of injection onto the trans-lunar trajectory are possible. For this reason, a specific set of trajectory characteristics was selected for plotting. The procedure in each case was to begin with the final point on the trajectory with a velocity normal to the lunar surface at the given α and β . The trajectory was then propagated backward in time until it either encountered the Earth or the Moon, or the trajectory duration reached 200 days. For those trajectories not encountering the Earth or the Moon in this time period, a search was then made for the periaipse closest to the Earth. Several quantities were then computed using the point at encounter or periaipse. They included the periaipse radius relative to the Earth, the TOF, the

launch energy (C_3), and inclination in the Earth Mean Equator and Equinox of J2000 (EME2000) frame.

Results showing the origin of each trajectory encountering the Moon are given in Fig. 5-11. For these cases three-dimensional effects are included, and it is now possible for the trajectory to miss encounters with the Earth and Moon by traveling above or below them. A significant number of encounters are still observed though, and the features seen for the $\theta = 0$ cases in the planar model may still be observed here where β is 0 deg. Although a significant number of Earth-origin trajectories are observed for low Jacobi constants, as the Jacobi constant increases (energy decreases), the number of Earth–Moon transfers decreases. Once a Jacobi constant of 2.8 is reached, there are no more of these types of trajectories in the Earth–Moon ephemeris model. However, there are still a significant number of Earth–Moon trajectories in the Sun–Earth–Moon ephemeris model. Indeed, a significant number still exist as the Jacobi constant is increased, even above 3.1. As in the planar case, the Sun may be thought of as changing the energy or Jacobi constant of the trajectory while the velocities at the Moon remain the same in each model. This observation emphasizes the need to include the Sun’s influence in the trajectory design process, but it raises the question as to what types of Earth–Moon trajectories exist at these energies and how long are their times of flight? It is difficult to answer these questions completely since trajectories are constantly changing with energy, but it is interesting to observe some of the trajectories that exist in the Sun–Earth–Moon system with no corollary in the Earth–Moon system. Two sample trajectories from the line of Earth origin trajectories at $C = 2.6$ that do not exist in the Earth–Moon system are given in Fig. 5-12. The majority of cases found in this line are similar to the trajectory in Fig. 5-12(a), and they exhibit the characteristics of known trajectories designed to utilize the dynamics of the invariant manifolds of libration orbits. They approach the L_1 Lagrange point from the Earth in the Sun–Earth system and then fall away toward the Moon. Although almost all of the trajectories follow this type of orbit, some do have characteristics similar to the trajectory in Fig. 5-12(b). In this case, the Sun’s gravity is still influential, but an intermediate flyby is inserted.

It is also interesting to observe the types of trajectories that exist for higher Jacobi constants, or lower velocities, at the lunar surface in the Sun–Earth–Moon system where no analogues in the Earth–Moon system have been found. Several samples are shown along with the trajectory origin plots in Fig. 5-13 to provide an overview of these types of trajectories. Here, an interesting phenomenon occurs. As the Jacobi constant increases to 3.0, the trajectories originating at the Earth are scattered across the map. The majority of the Earth-origin trajectories seem to require multiple flybys of the Earth or the Moon. The sample trajectories shown in Fig. 5-13(a) are intended to be representative of the types of trajectories found across the map. Although a few trajectories, such as those found in the lower left corner of the map, utilize the libration dynamics more directly, the majority seem to require variations on different phasing flybys as shown by the various trajectories. As the Jacobi constant is increased further to a value of 3.1 in Fig. 5-13(b), a line of trajectories appear. These trajectories, as shown in the figure, once again utilize the libration orbit dynamics more directly, sometimes making use of a single flyby along the trajectory. The remaining scattered

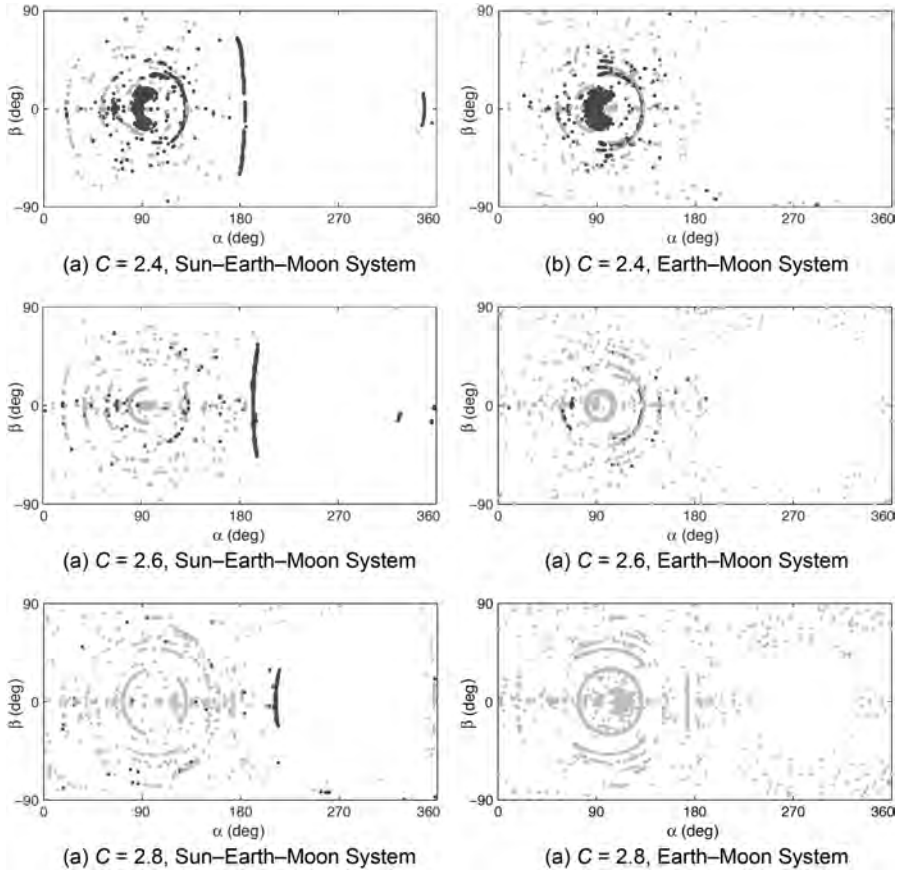


Figure 5-11 Plots showing the origin of the spatial collision trajectories. Black indicates the trajectory originated at the Earth, and gray indicates it originated at the Moon. If it is white, no encounter occurred within 200 days (for epoch of January 1, 2015) [192] (Copyright © 2011 by American Astronautical Society Publications Office, San Diego, California (Web Site: <http://www.univelt.com>), all rights reserved; reprinted with permission of the AAS, 2006)

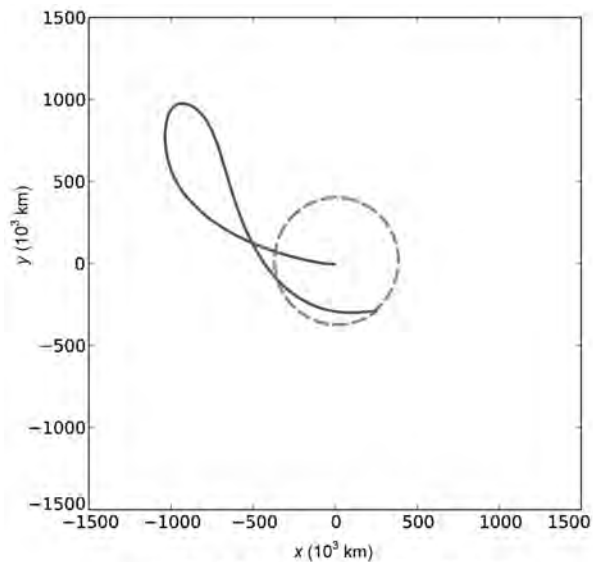
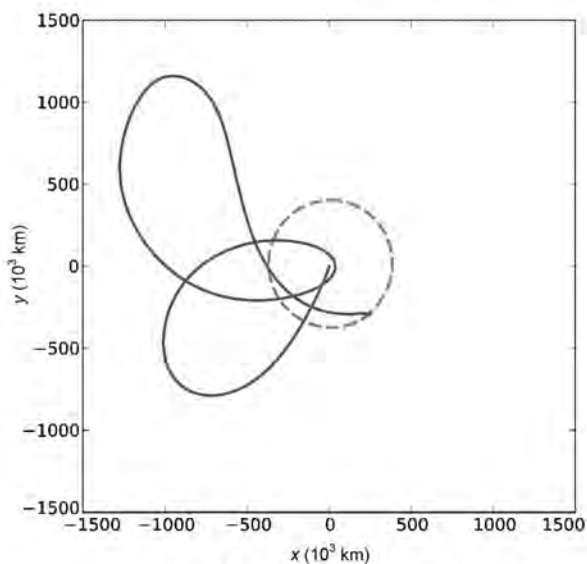
(a) $C = 2.6$, $\alpha \approx 194.5$ deg, $\beta \approx -32.0$ deg(b) $C = 2.6$, $\alpha \approx 194.5$ deg, $\beta \approx -10.0$ deg

Figure 5-12 Sample trajectories at $C = 2.6$ for the Sun–Earth–Moon system. The trajectories correspond to the line of trajectories not found in the Earth–Moon plots [192] (Copyright © 2011 by American Astronautical Society Publications Office, San Diego, California (Web Site: <http://www.univelt.com>), all rights reserved; reprinted with permission of the AAS).

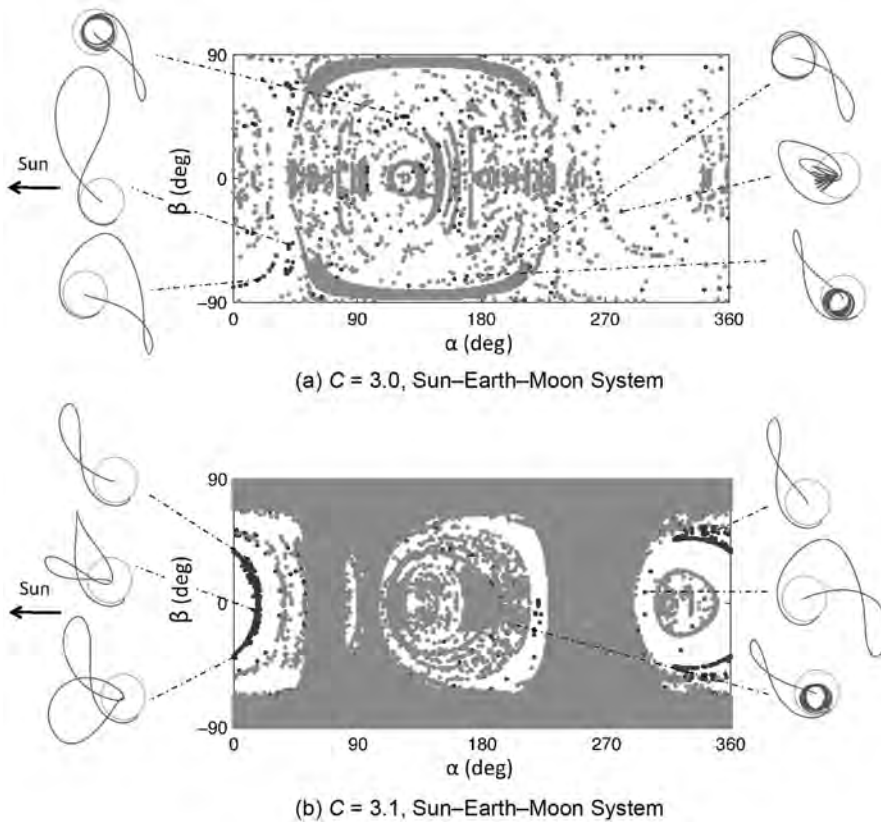


Figure 5-13 Plots showing the origin of the spatial collision trajectories. Black indicates the trajectory originated at the Earth, and gray indicates it originated at the Moon. If it is white, no impact occurred within 200 days. Trajectories are shown for select points in the Earth-centered Sun–Earth rotating frame. The gray circular orbit is the Moon’s orbit while the Sun is in the indicated direction. The scale is the same for all trajectories shown, and the trajectories all originate at the Earth [192] (Copyright © 2011 by American Astronautical Society Publications Office, San Diego, California (Web Site: <http://www.univelt.com>), all rights reserved; reprinted with permission of the AAS).

trajectories found near the center of the plot continue to use multiple gravity flybys to connect the Earth and the Moon.

Another interesting characteristic to include in the analysis is the TOF required for each trajectory originating at the Earth. More specifically, what are the minimum TOF values that may be achieved at each energy? The TOF values provide an indication of whether the trajectories at each Jacobi constant fall more in the category of direct transfers, low-energy transfers, or somewhere in between. The existence

of trajectories in the Sun–Earth–Moon system that do not exist in the Earth–Moon system already indicates the presence of trajectories utilizing multi-body effects that would be expected to fall more in the low-energy category. The minimum TOF values for selected Jacobi constants are listed in Table 5-1. These values were computed using a grid with the points spaced at one-degree intervals in each variable. As expected, the TOFs start near the 3-day values seen for the Apollo program’s direct transfers for a Jacobi constant of 2.2, and climb to over 100 days for a Jacobi constant of 3.0. It is surprising though that the minimum TOF at a Jacobi constant of 3.1 drops to 78.7 days. Although this point is lower than most of the others at this energy, a number of trajectories still exist in the 90-day time range. The reasons behind this drop in the TOF may be more clearly understood by reexamining the typical trajectories plotted for the Jacobi constants of 3.0 and 3.1 in Fig. 5-13. As mentioned previously, the majority of the trajectories computed for the Jacobi constant of 3.0 required multiple phasing flybys, while the $C = 3.1$ trajectories typically utilize the libration dynamics without these phasing loops. This phenomenon would explain the lower minimum TOF value at $C = 3.1$, since many of the trajectories at this energy actually use a more direct approach.

The analysis so far has focused on categories of trajectories originating at the Earth, with the expectation that trajectories from a given category may often be modified to meet the particular requirements of a mission when they are supplied. Often, however, trajectories that originate within some distance of the Earth may be used by targeting them from low Earth orbit. It is also important to quantify the orbital parameters of the initial conditions of the analyzed trajectories relative to the Earth in order to determine the suitability of the trajectories for particular missions. For example, if a launch from Cape Canaveral is selected, an inclination relative to the Earth’s pole of 28.5 deg would be desirable. Particular quantities relevant to mission design are presented next with the objective of presenting an overview of the possible trajectories so that initial estimates may be made for future mission design.

Table 5-1 Minimum TOF values from the computed trajectories originating at the Earth for selected Jacobi constants.

C	TOF (days)
2.2	3.4
2.4	29.8
2.6	58.3
2.7	57.8
2.8	74.0
2.9	94.9
3.0	101.0
3.1	78.7

The analysis here focuses on the Sun–Earth–Moon system so as to encompass the complete range of trajectories.

The closest periaipse values obtained over 200 days for selected Jacobi constants in the Sun–Earth–Moon system are plotted in Fig. 5-14. Note that some of the gaps in (a) are Earth intersection trajectories as can be seen by reexamining Fig. 5-13. It can

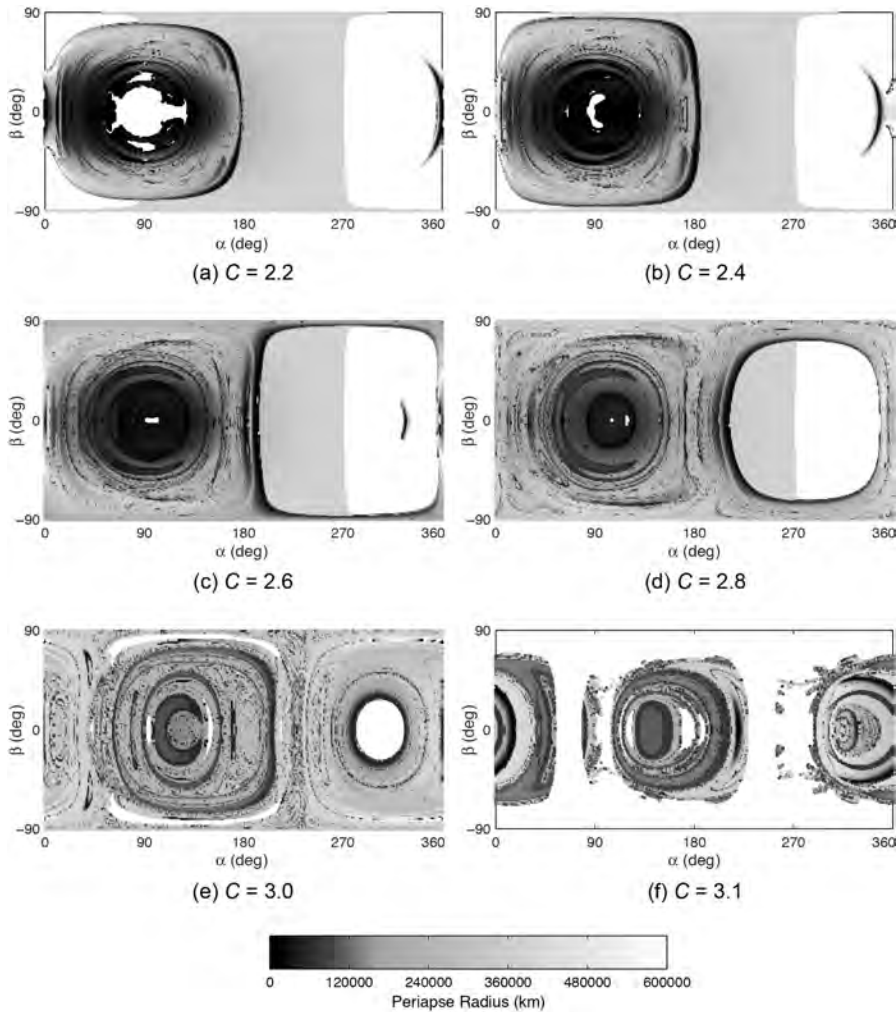


Figure 5-14 Periaipse radius values for the computed trajectories plotted over the surface for a range of Jacobi constant values [192] (Copyright © 2011 by American Astronautical Society Publications Office, San Diego, California (Web Site: <http://www.univelt.com>), all rights reserved; reprinted with permission of the AAS).

immediately be seen from the plots that the majority of the trajectories never come near the Earth. In general, the trajectories originating near $\alpha = 90$ deg produce the most trajectories with periapses closer to Earth. This does shift with Jacobi constant, as was seen in the earlier Europa study [199]. As the Jacobi constant increases and energy decreases, it appears that fewer trajectories come as close to the Earth, but the majority stay near the system. The chaos present in the system can especially be observed for $C = 3.0$, where trajectories very close to each other alternate with low and high periapses.

From the analysis so far, it appears that a large portion of the lunar surface may be physically accessible to trajectories coming from the Earth or near the Earth, but the feasibility of flying these trajectories will depend on mission design parameters such as TOF, launch energy (C_3) at Earth, and inclination. It is uncertain what two-body orbital element parameters (such as C_3 and inclination) mean when they are computed where multi-body perturbations are significant, but this problem may be alleviated by computing these parameters where multi-body effects are minimized. With this objective in mind, only parameters for trajectories with periapses lower than geosynchronous radius are plotted in the following figures. For these plots, the parameters are now included for those trajectories originating at the Earth, and in those cases their values are computed using the initial conditions at the Earth's surface.

The TOFs and C_3 values are plotted in Fig. 5-15 for those trajectories with periapsis relative to the Earth of less than geosynchronous radius. The immediate feature that can be noticed is the sparsity of points compared to the previous plots, confirming that a large number of trajectories ending at the lunar surface never come near the Earth. Indeed, for lower Jacobi constants, the locations between approximately 180 deg and 360 deg have almost no trajectories originating near the Earth. Curiously, around a Jacobi constant of 3.0, the trajectories are more randomly distributed across the surface with a combination of C_3 values. This feature may be partly explained by returning to the TOF values. From the plots, it can be confirmed that the minimum TOFs generally increase with Jacobi constant. The minimum TOF values at $C = 3.0$ are significantly larger, indicating that low-energy trajectories under the influence of chaos are beginning to be more common. Given the variety of trajectory types and the TOFs involved, it is not surprising that more of the lunar surface is potentially covered. Examining the trends in the TOF plots, it may also be observed that longer TOF trajectories appear to exist at each energy level. The lines of long TOF trajectories correspond to low-energy trajectories using the Sun's perturbations and approaching the libration points of the Sun–Earth system. It is also worth noting that a variety of C_3 options are available at each energy level for transfers to the Moon. Even for low Jacobi constants, there still exist some relatively low C_3 options, although the minimum is higher than that found for the higher Jacobi constant cases. It is important to realize that a small change in the landing location can result in a drastic change in the required C_3 even with similar TOFs and the same velocity at the Moon. This fact is important for mission designers, as it may sometimes be possible to move the landing site slightly to improve ΔV , or a similar effect may be obtained by targeting with maneuvers along the trajectory. Trajectory correction maneuvers may

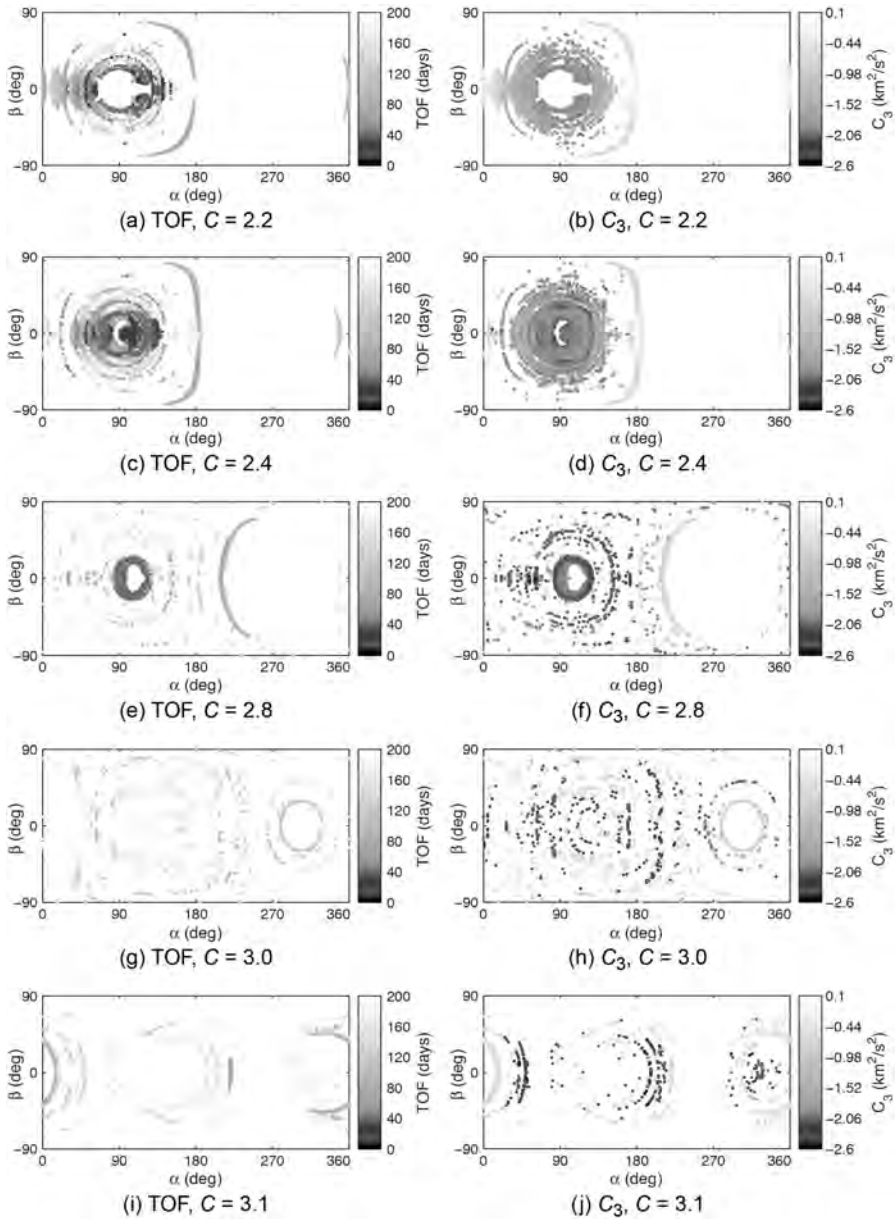


Figure 5-15 TOF and C_3 for each trajectory plotted over the surface for a range of Jacobi constants [192] (Copyright © 2011 by American Astronautical Society Publications Office, San Diego, California (Web Site: <http://www.univelt.com>), all rights reserved; reprinted with permission of the AAS).

also help aid in reducing the ΔV . In general, it is useful to be aware of the chaotic nature of the design space as seen from these plots.

Finally, it is important for most mission designs to consider the inclination. The inclination results in the EME2000 coordinate frame are given in Fig. 5-16. One of the important features to notice here is that a variety of inclinations are possible. A choice of trajectories exist with the lower inclinations suitable for launch from Cape

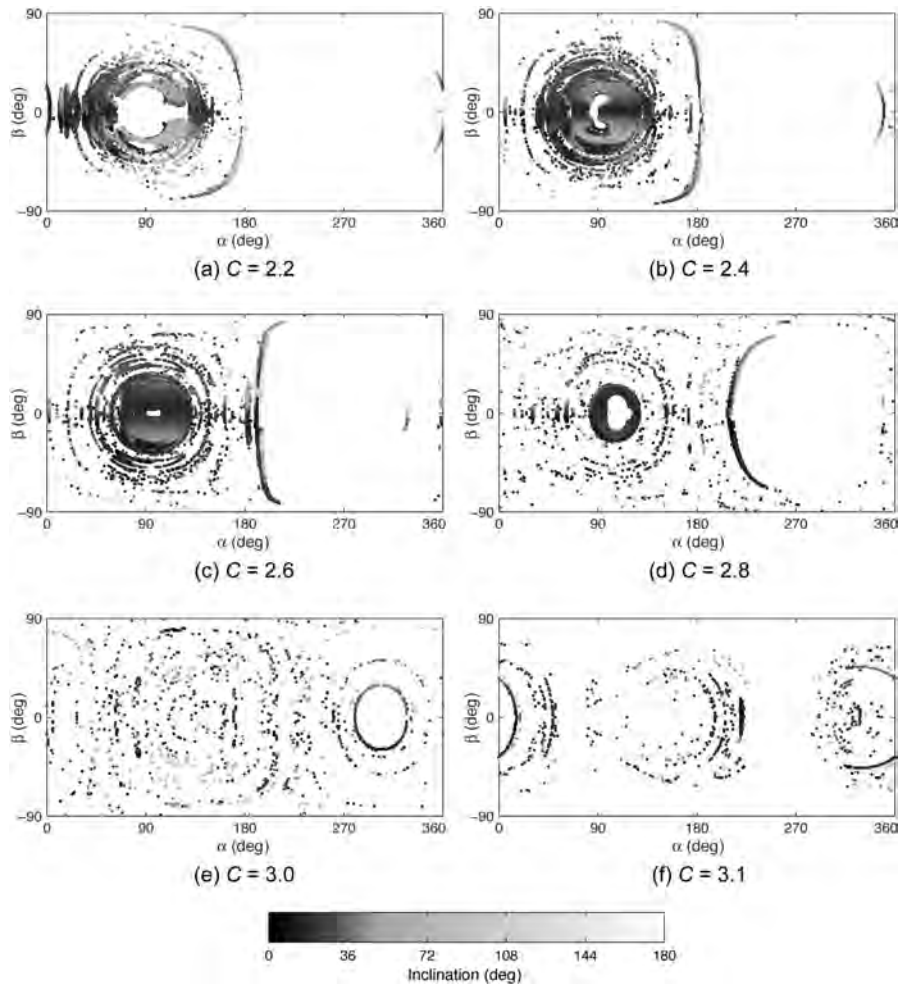


Figure 5-16 Inclination computed relative to the Earth in the EME2000 coordinate frame [192] (Copyright © 2011 by American Astronautical Society Publications Office, San Diego, California (Web Site: <http://www.univelt.com>), all rights reserved; reprinted with permission of the AAS).

Canaveral. The particular inclinations needed for a mission will depend on the target location on the Moon and the particular constraints of the mission. They are provided here as a sample of the range of the values that are possible.

5.5.2 Trajectories Arriving at Various Angles to the Lunar Surface

The planar CRTBP provides a convenient framework in which to understand and visualize the relationship between invariant manifolds and lunar approach trajectories, but the design of real-world equivalent trajectories often requires a landing at either higher or lower latitudes. Indeed, many of the recently proposed landing sites at the Moon are at northern or southern latitudes [204], and one of the locations that is currently a focus for a lunar lander is more southern latitudes in the Aitken Basin. In this analysis, lunar landing trajectories are analyzed over the three-dimensional surface of the Moon, and the approach geometry of the trajectories in three dimensions is also analyzed.

The landing geometry of trajectories traveling from the Earth to the Moon is of particular importance for mission design. In the previous section and in Anderson and Parker [192, 195] we analyzed trajectories encountering the Moon normal to the surface to determine whether these trajectories originated at the Earth within the previous 200 days. Given this elevation angle constraint, only some locations of the Moon's surface were found to be accessible from the Earth. For this analysis, trajectories were allowed to approach each point on the lunar surface from all directions. These directions were specified relative to the surface at each point. The azimuth angle (Ω) is measured clockwise from north where north is the lunar orbit's North Pole, rather than the Moon's North Pole, to be consistent with the results from the CRTBP. The elevation angle (ϕ) is measured positive above the Moon's surface, with a trajectory encountering the Moon's surface normal to the surface having an elevation angle of 90 deg. (Note that this is different from θ used for the planar case, but it was chosen to be more consistent with typical mission design parameters.) While the previous analysis was ideal for impactors, the trajectories computed here are applicable for a wide range of mission types traveling to the lunar surface. Additional parameters for each trajectory related to the original characteristics relative to the Earth may be computed, but the focus here is on characterizing the approach geometry. For the following analysis the trajectories were computed over the surface of the Moon using 1-deg increments in α and β . The same definition is used for α that is used in the planar problem in Fig. 5-3. As described earlier, β is measured like latitude and is positive above the xy plane. Two different grids were used for the azimuth and elevation angles. In each case, the elevation angle was varied in even increments, and the steps taken in azimuth angle were specified initially for an elevation angle of 0 deg. The number of azimuth points were then decreased with $\cos(\phi)$ so that the number of points decreased with elevation angle. Both a fine grid and a coarser grid were used in this analysis. For the fine grid case, 1-deg increments were taken at 0-deg elevation for Ω , and 1-deg increments were used for elevation. For the coarser grid, 10-deg increments were used for Ω at 0-deg elevation, and 3-deg increments were used for elevation. This coarser grid was found to provide a good approximation

that conveyed the overall trends of the fine grid, while allowing for a more reasonable computation time. Even with this coarser grid, computing trajectories over the entire surface in the ephemeris problem for each Jacobi constant required approximately seven days running in parallel on 40 processors. Unless otherwise stated, this coarser grid is the one used throughout the analysis.

As an initial step in the analysis, the set of trajectories was computed in the CRTBP for a Jacobi constant of 2.6. The trajectories were computed for both the fine grid and the coarser grid. Comparing the maximum and minimum elevation angles resulted in trajectories that originate at the Earth as shown in Fig. 5-17. Using the symmetry about the xy plane mentioned earlier, it can be seen that the northern and southern latitudes will be reflected for the elevation plots in the CRTBP. Note that the azimuth angles would need to account for the reflection if they are

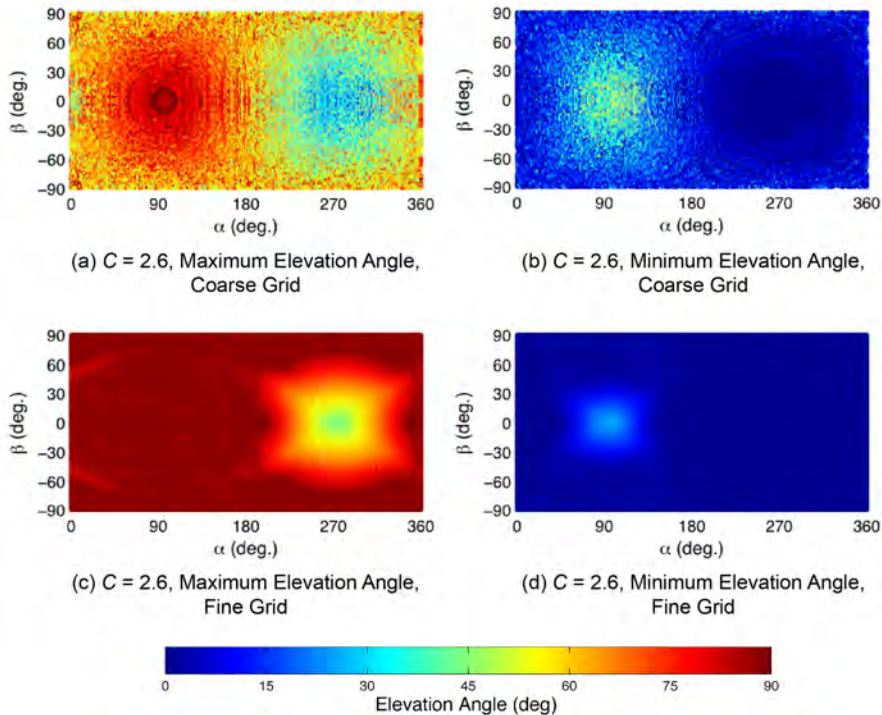


Figure 5-17 Maximum and minimum elevation angles for trajectories originating at the Earth and encountering the Moon at each point on the surface. These cases are computed in the CRTBP for $C = 2.6$. Results from two different grids (in elevation and azimuth angle) are shown [193] (Copyright © 2011 by American Astronautical Society Publications Office, San Diego, California (Web Site: <http://www.univelt.com>), all rights reserved; reprinted with permission of the AAS). (See insert for color representation of this figure.)

plotted, and although similar results would be expected in the ephemeris problem, the variations in the ephemeris require that the northern and southern hemispheres be computed independently. Using this symmetry the values computed for the northern and southern hemispheres were reflected in Fig. 5-17 to save computation time. By comparing the plots, it can be seen that, as might be expected, the finer grid captures more trajectories at higher and lower elevation angles that originate at the Earth, however, the overall trends in the data remain the same for both grids. In each case the range of elevation angles from minimum to maximum is shifted higher near $\alpha = 90$ deg and lower near $\alpha = 270$ deg. Referring back to Fig. 5-3, the 90-deg direction corresponds to the leading edge of the Moon, and the 270-deg direction to the trailing edge. The coarser grid is used in the remainder of this analysis, so it should be remembered that details in the plots may change with a finer grid, but the overall trends can still be observed.

An analysis of trajectories for a Jacobi constant of $C = 2.8$ confirmed our earlier result for trajectories encountering the Moon normal to the surface of the Moon that no Earth-return trajectories were found for this Jacobi constant or higher ones in the CRTBP. However, it is expected that Earth-origin trajectories with velocities consistent with higher Jacobi constants in the CRTBP will exist in the ephemeris problem because these trajectories may use the Sun's perturbations to travel from the Earth to the Moon. Those higher Jacobi constants, especially those approaching the values near C_{L_1} and C_{L_2} are especially relevant for the computation of the invariant manifolds of libration point orbits, which is useful for the comparison later in this study. The elevation angle range results are shown in Fig. 5-18 for Jacobi constants ranging from $C = 2.6$ to 3.1 in the ephemeris problem. Note that, as in Anderson and Parker [192, 195], the Jacobi constant for the ephemeris plots is used as a shorthand for a particular set of velocities computed around the Moon in the CRTBP. These same velocities are attached to the Moon in the ephemeris problem referenced to the instantaneous orbital plane of the Moon's orbit around the Earth. The symmetry used to simplify the computations in the CRTBP is no longer present for the ephemeris problem, and trajectories were directly computed for the entire plot. Once the trajectory is integrated backward from the Moon, the Jacobi constant of the trajectory will vary in both the Earth-Moon and Sun-Earth systems.

Comparing the results from Fig. 5-17 for the Jacobi constant case of 2.6 in the CRTBP and the ephemeris problem results reveals that they are quite similar. The maximum and minimum elevation values still occur at approximately the same locations on the surface for each case. However, several new bands of high-elevation-angle cases occur for the ephemeris case near $\alpha = 180$ deg for the maximum elevation angle case and from approximately $\alpha = 290$ deg to 360 deg. Additional bands also seem to exist for the minimum elevation angle case, especially for high and low latitudes. It is natural to expect from past work that these bands may represent trajectory options that exist as a result of the Sun's influence, and it is interesting that these types of bands remain up through $C = 2.8$ (Figs. 5-18(a) through 5-18(d)). An interesting topic planned for future study is to determine how these characteristics vary with a finer grid. However, the comparison performed here is with the same grid in each case, indicating that these additional trajectories exist.

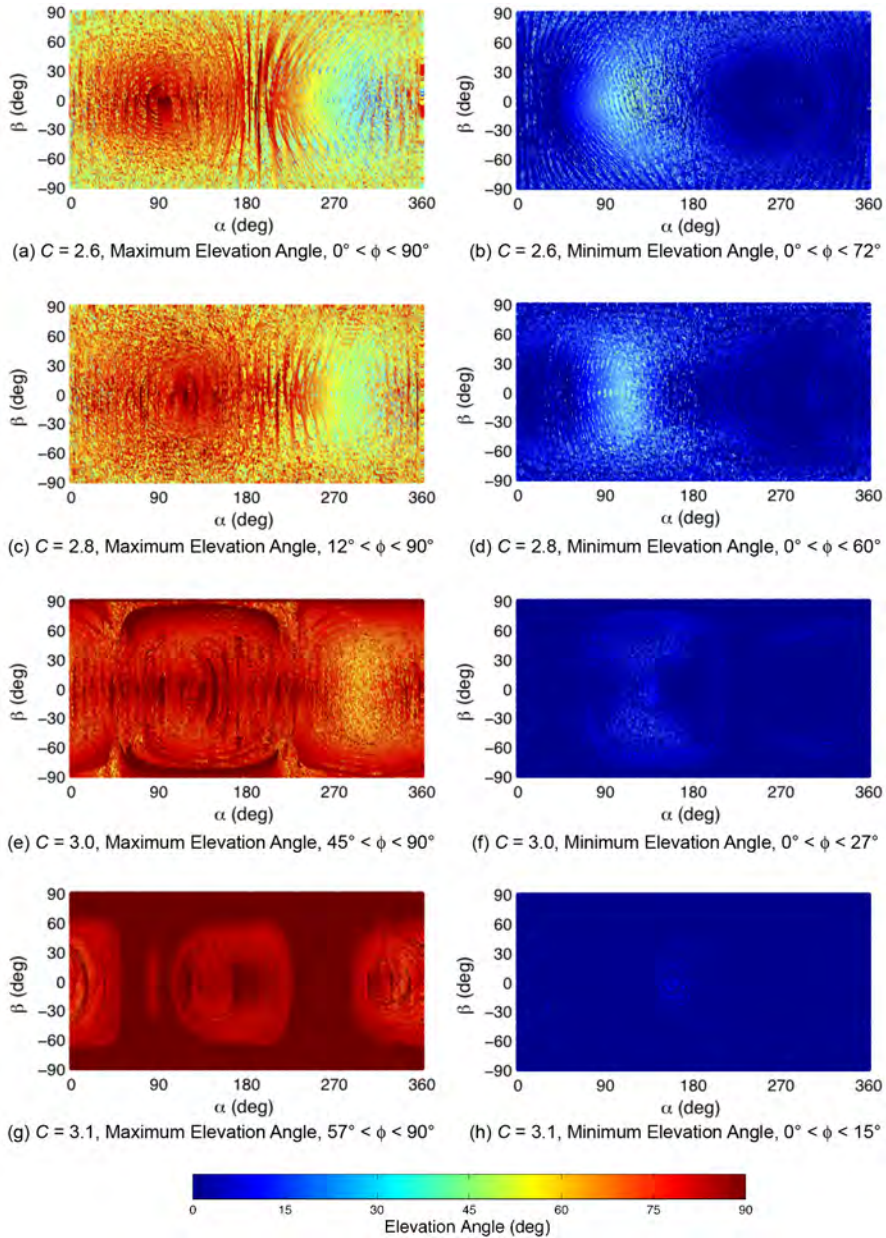


Figure 5-18 The minimum and maximum elevation angles of trajectories originating at the Earth for each point on the lunar surface. These trajectories are computed in the Earth–Moon ephemeris system including the Sun’s perturbations [193] (Copyright © 2011 by American Astronautical Society Publications Office, San Diego, California (Web Site: <http://www.univelt.com>), all rights reserved; reprinted with permission of the AAS). (*See insert for color representation of this figure.*)

As the Jacobi constant increases even more as seen in Figs. 5-18(e) through 5-18(h), the range of elevation angles for lunar landing at each point seems to increase even more. The location of the peaks also seems to shift, and for the maximum elevation angle plots, the peaks move to the right or eastward with increasing Jacobi constant. When a Jacobi constant of 3.1 is reached, the maximum elevation angle for points containing a trajectory originating at the Earth never drops below 57 deg, and the minimum elevation angle for the same points never goes over 15 deg. It is important to mention that although the points look dense across the surface in the plots, this is because of the size of the plot and the points used for plotting. There are individual points on the surface where no Earth-origin trajectory exists for this grid, but there are always nearby points where such a trajectory exists. For real-world mission design, a small ΔV can be used to target slightly different points, and the surface of the Moon is covered in practice for mission design purposes. It has also been found for particular points that if a much finer grid is used, typically some Earth-origin trajectories are found, and these points will be included in future studies. The points with no Earth-origin trajectories for this grid are not included in the elevation angle ranges listed in the plots. These results for higher Jacobi constants agree generally with the normal trajectory cases seen in our previous work [192, 195]. The additional range of geometries available for landing at these energies appears to be a result of the increasingly chaotic nature of the system as the Jacobi constant approaches the values at the L_1 and L_2 libration points. In other words, the trajectories are more able to take advantage of chaos to arrive at different elevation and azimuth angles. This also indicates that these Jacobi constants are of particular interest for comparison with the invariant manifolds of libration orbits. One interesting statistic to examine with a fixed grid is the maximum number of trajectories at a particular point that originate at the Earth. Although this number is generally quite low, there are some points where it peaks. The maximum number of trajectories at a particular point is listed in Table 5-2 for different Jacobi constants. The higher values are found for a Jacobi constant of 2.6 and 3.1. The $C = 2.6$ results include more direct trajectories that still exist in the CRTBP and do not require the Sun's influence, and the $C = 3.1$ results include those trajectories that are heavily influenced by the Sun. The total number of Earth-origin trajectories follows the same trend. These numbers

Table 5-2 Maximum number of Earth-origin trajectories at a single point on the lunar surface for a fixed grid including the corresponding location and the total number of Earth-origin trajectories for various values of Jacobi constant.

Jacobi Constant	Maximum at a Point	Location (α, β)	Total Number
2.6	27	(193 deg, -36 deg)	290,672
2.8	16	(213 deg, -18 deg)	114,684
3.0	14	(225 deg, -11 deg)	162,061
3.1	36	(192 deg, 7 deg)	298,621

are a function of the grid that is being used and can be refined by using a denser grid; however, they do align with the results from the trajectories computed normal to the lunar surface seen in our earlier work.

Because the trajectories are computed in the ephemeris problem for the cases just discussed, the results will naturally vary with the initial epoch of the integration. A sample of the results was computed for four different epochs around the Moon's orbit (with the time intervals each at approximately one-quarter of the Moon's orbit) to determine how they might vary with the initial epoch. Representative results for a Jacobi constant of 2.8 are shown in Fig. 5-19. The salient features of the plots remain generally the same for each epoch in that the maximum values still occur near $\alpha = 90$ deg and the minimum values occur near $\alpha = 270$ deg. The January 7 and 21 cases have more locations with higher elevation angles, especially near $\alpha = 270$ deg, mixed in with lower elevation angle points. These two cases appear better positioned to take advantage of the Sun–Earth libration point dynamics, which could increase

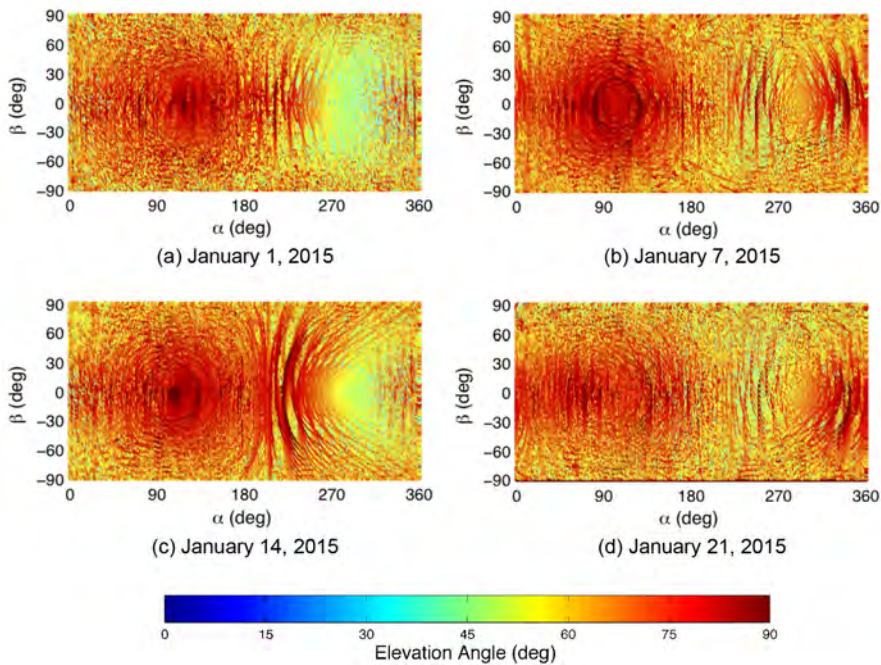


Figure 5-19 Comparison of maximum elevation angle results around the lunar orbit at seven day intervals for $C' = 2.8$ [193] (Copyright © 2011 by American Astronautical Society Publications Office, San Diego, California (Web Site: <http://www.univelt.com>), all rights reserved; reprinted with permission of the AAS). (See insert for color representation of this figure.)

the range of elevation angles that may be obtained for approaching the Moon. Overall though, given this comparison, it is expected that the results from this study may be extrapolated to other epochs without drastically changing the outcome.

Another important aspect of the approach for mission design is, of course, the azimuth angle of the trajectory. Plotting this information in a global sense is difficult, but a sample of the types of results obtained for each Jacobi constant may be visualized in Fig. 5-20 for a subset of the points. The azimuth angles are plotted for each point on a grid computed at 30-deg intervals in both α and β . For these plots, the fine grid was used at each point on the surface (which of course produced more trajectory options), and the trajectories were limited to those with $C_3 < 0.0 \text{ km}^2/\text{s}^2$ at the Earth. The orientation of the lines centered on each point indicates the azimuth angle, and the color is used to designate the corresponding elevation angle of each trajectory. Note that the ± 90 -deg cases used azimuths that were rotated differently at each elevation as a result of the transformation used to compute them. So the specific results differ, but they generally show similar trends. It is interesting that there are definite regions

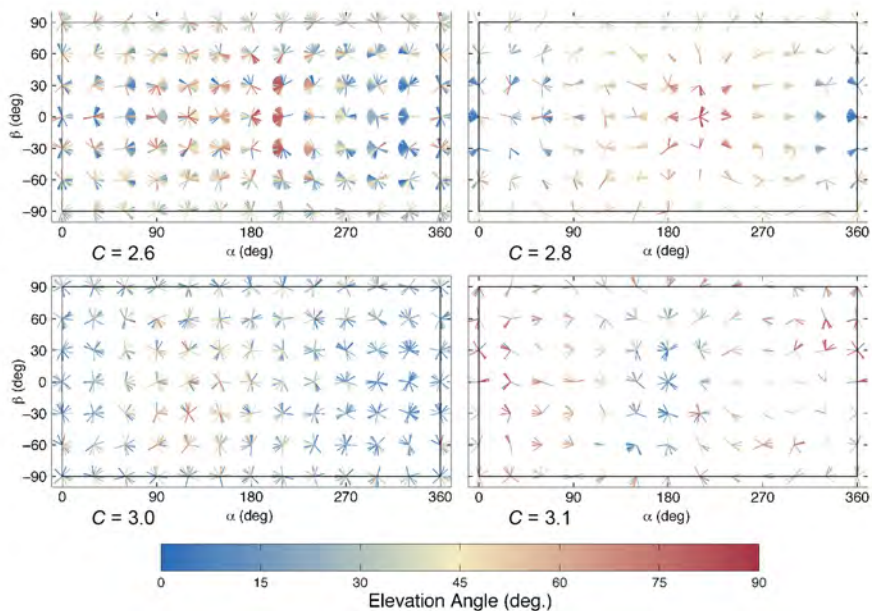


Figure 5-20 Azimuth angles at points on a 30-deg grid on the lunar surface. The plotted lines at each gridpoint are oriented in the proper azimuth direction for each individual trajectory. The color corresponds to the elevation angle of that trajectory. The trajectories shown here are limited to those with $C_3 < 0.0 \text{ km}^2/\text{s}^2$ at the Earth [194] (first published in Ref. [194]; reproduced with kind permission from Springer Science+Business Media B.V.). (*See insert for color representation of this figure.*)

where the majority of Earth-origin trajectories appear to have similar elevation angles. In each case though, there are often just a few high or low trajectories that result in the extremes seen in the elevation angles plots. This fact is worth keeping in mind for mission design since a particular elevation angle may be available in combination with only a few azimuth angles. In general it appears that higher-elevation options are more available as the Jacobi constant increases, although there are typically at least a few low elevation angle options at each point. The combinations of available elevation and azimuth angles are evaluated in more detail for $C = 3.1$ in the following comparison with invariant manifolds, which helps explain the features seen in these plots a little more directly. In general, these plots can provide a broad overview of the available trajectory options.

5.6 TRANSFERS BETWEEN LUNAR LIBRATION ORBITS AND THE LUNAR SURFACE

A general framework and understanding does exist in regard to the relationship between invariant manifolds of unstable orbits and the Moon. (Refer to Section 2.6.10 for more background on invariant manifolds.) Much of the work to design low-energy trajectories from the Earth to the Moon has focused on the use of libration point orbits along with their stable and unstable manifolds [39, 45, 51, 203]. Koon, Lo, Marsden, and Ross examined this problem for the planar case [37], and Parker studied approach cases to lunar libration orbits using invariant manifolds in his dissertation [46]. Baoyin and McInnes analyzed some specific cases of transfers from libration points and planar Lyapunov orbits to the lunar surface [205]. In particular, they searched for the Jacobi constant that would provide complete coverage of the lunar surface by the invariant manifolds of the selected Lyapunov orbit. Von Kirchbach et al. [201] looked at the characteristics of the invariant manifolds of a Lyapunov orbit as they intersected the surface of Europa in the context of the escape problem. Alessi, Gómez, and Masdemont [206] examined the locations of the Moon reachable by the stable manifolds of a range of halo orbits and square Lissajous orbits. They computed the intersections of these invariant manifolds with the surface of the Moon with the expectation that they could be used for astronauts to escape to a libration point orbit if necessary. Anderson [207] examined the approach problem within the context of the invariant manifolds of unstable resonant and Lyapunov orbits as the trajectory ties into the resonances of the Jupiter–Europa endgame problem following invariant manifolds [158, 208–210].

One focus of the transfer to the lunar surface using invariant manifolds is on the final approach from a desired libration orbit to the lunar surface. The problem may be most easily approached using the planar CRTBP and Lyapunov orbits. Two sample Lyapunov orbits found in Anderson and Parker [192, 195] are replotted here in Fig. 5-21. The Jacobi constants for these orbits were chosen so that the invariant manifolds of the Lyapunov orbits just graze the surface of the Moon. The Jacobi constants where the Lyapunov orbits cover the surface of the Moon were computed

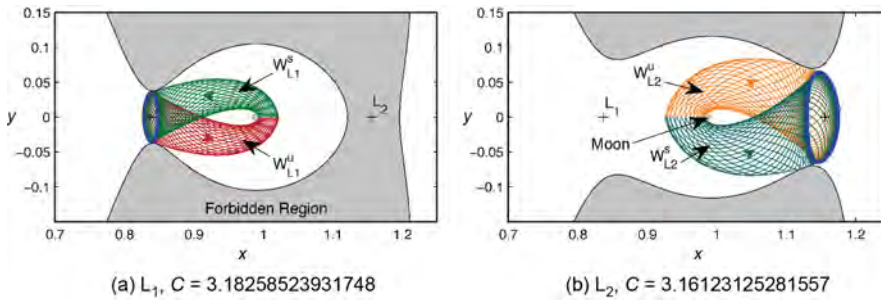


Figure 5-21 Invariant manifolds of libration orbits computed for Jacobi constants where the manifolds are tangent to the surface of the Moon [193] (Copyright © 2011 by American Astronautical Society Publications Office, San Diego, California (Web Site: <http://www.univelt.com>), all rights reserved; reprinted with permission of the AAS). (*See insert for color representation of this figure.*)

by Baoyin and McInnes [205] as approximately $C = 3.12185282430647$ for an L_1 Lyapunov orbit and $C = 3.09762627497867$ for an L_2 Lyapunov orbit.

As a first step in the comparison, the lunar landing geometry of the invariant manifolds of various halo orbits is analyzed. Alessi, Gómez, and Masdemont [206] examined similar trajectories for escaping the surface of the Moon to various halo orbits and summarized the areas on the Moon from which such escape trajectories are possible. We are concerned here with a combination of the landing location along with the landing geometry, therefore, a similar technique to that used in Fig. 5-20 is employed here. In subsequent figures, the intersections of the unstable manifolds of the L_1 halo orbits are indicated by a red point, and the intersections for the L_2 halo orbits are orange points. The azimuth angle and the elevation angle are indicated by the direction and the color of the line segments, respectively.

The results for a halo orbit at $C = 3.1$ are shown in Fig. 5-22. It can be immediately seen that for this energy, the L_1 halo orbit invariant manifolds generally fall on the leading edge of the Moon in its orbit, and the L_2 halo orbit invariant manifolds fall on the trailing edge of the Moon. As expected, the intersections of the northern and southern halo orbits are reflected about $\beta = 0$. The elevation angles are somewhat lower for the L_1 halo orbits than the L_2 halo orbits. All together, the unstable manifolds provide relatively broad coverage of much of the lunar surface, although significant regions are still not intersected by the invariant manifolds. This may be remedied by examining the invariant manifolds at additional energies. The unstable manifold intersections with the Moon can change significantly with the Jacobi constant as can be seen for the intersections plotted with a Jacobi constant of 3.08 in Fig. 5-23. The intersections for the L_1 case have divided into two different regions, and the L_2 intersection case has grown tighter together. It should be reiterated that the unstable manifold intersections can increase if larger time intervals are used for

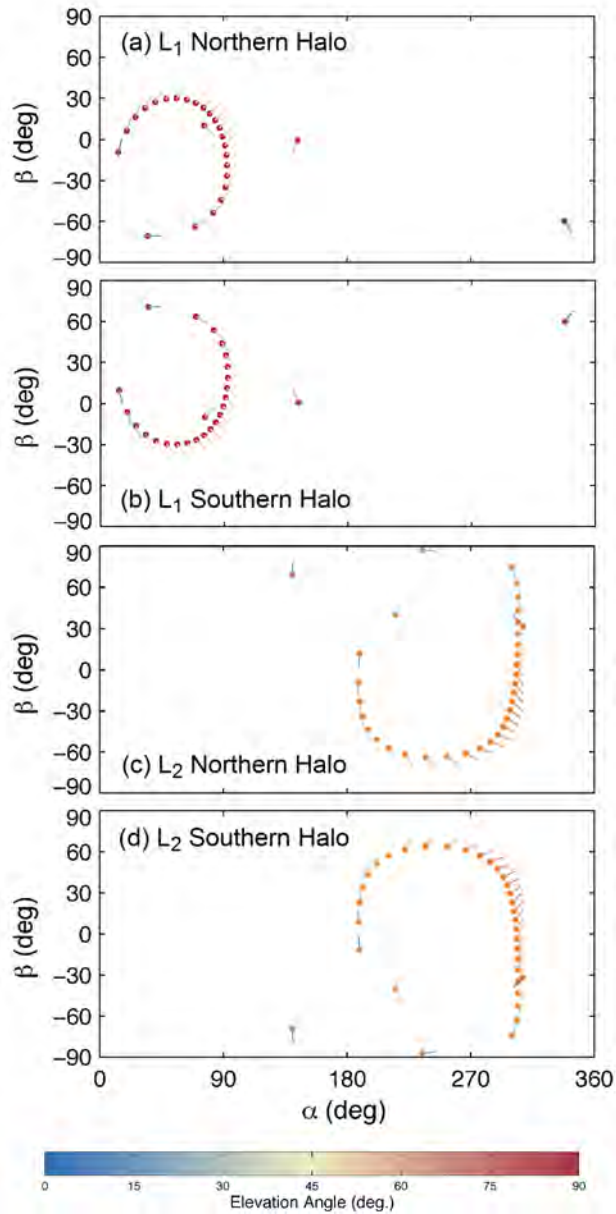


Figure 5-22 Unstable manifold intersections of the specified orbits with the Moon for $C = 3.1$ [193] (Copyright © 2011 by American Astronautical Society Publications Office, San Diego, California (Web Site: <http://www.univelt.com>), all rights reserved; reprinted with permission of the AAS). (See insert for color representation of this figure.)

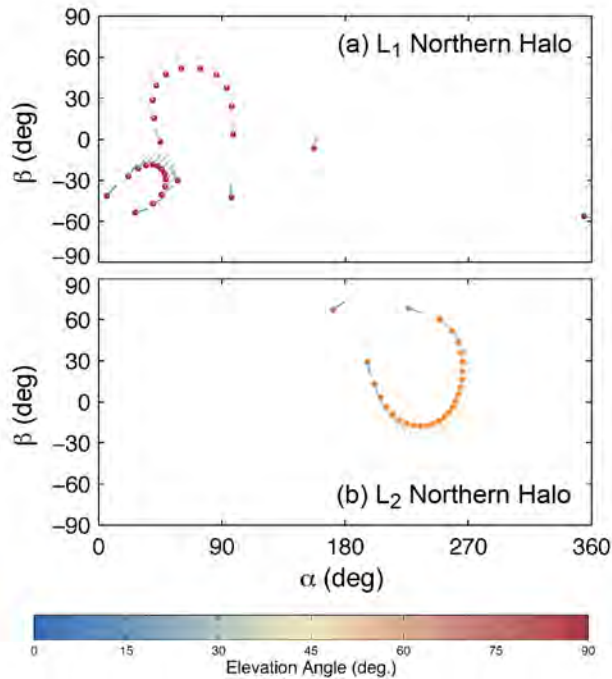


Figure 5-23 Unstable manifold intersections of the specified orbits with the Moon for $C = 3.08$ [193] (Copyright © 2011 by American Astronautical Society Publications Office, San Diego, California (Web Site: <http://www.univelt.com>), all rights reserved; reprinted with permission of the AAS). (See insert for color representation of this figure.)

the integration, and these plots focus on short-duration trajectories. The unstable manifold intersections also change even more as energy continues to change, but these energies appear to provide some of the most direct transfers.

This analysis shows that the unstable manifolds of halo orbits can provide broad coverage for landing at various points on the Moon, although not with the nearly complete coverage found from the previous results. It is also interesting to explore the relationship between the unstable manifolds and these Earth-origin trajectories from the general analysis. A similar examination to the one made for the planar problem would be desired, but the nature of the three-dimensional problem makes this drastically more complex. One possible method for performing this comparison is to examine the origin of the trajectories coming from all azimuth and elevation angles at each point that the unstable manifolds intersect the surface of the Moon. In this case, only one unstable manifold intersection is plotted for each location on the Moon relative to the trajectories coming in from all angles, but it still allows this point to be placed in context of the dynamics indicated by the source of each trajectory.

5.7 TRANSFERS BETWEEN LOW LUNAR ORBITS AND THE LUNAR SURFACE

Information about transfers from low lunar orbits to the lunar surface is provided in Section 4.6 on page 258.

5.8 CONCLUSIONS REGARDING TRANSFERS TO THE LUNAR SURFACE

A wide variety of trajectory options exist for transfer to the lunar surface. These range from more direct trajectories that may be primarily computed using just the influence of the Earth and Moon, to those at lower energies that require the influence of the Sun to compute. The invariant manifolds of libration orbits may be used for transfers to the lunar surface, and in combination with transfers to these libration orbits from the Earth, can be used as a complete transfer from the Earth. The trajectories computed for various Jacobi constants shown in the selected plots in this chapter may be used to obtain an initial idea of the types of trajectories available for different energy regimes. These energy regimes correspond to the constraints dictated by a particular mission, such as the available launch vehicle. Once the general type of trajectory that may be of interest is selected, more detailed initial guesses for particular trajectories may be obtained from the various plots showing trajectories coming in at various angles to the surface or from the invariant manifolds results. A mission designer may then modify and constrain these trajectories, while incorporating the mission design constraints of interest, to compute the final desired trajectory.